Title
Non-photolithographic plastic-mold-based fabrication of cylindrical and multi-tiered poly(dimethylsiloxane) microchannels for biomimetic lab-on-a-chip applications

Journal
RSC Advances, 5(122)

ISSN
2046-2069

Authors
Jang, Minjeong
Kwon, Young Jik
Lee, Nae Yoon

Publication Date
2015

DOI
10.1039/c5ra22048c

Peer reviewed

RSC Advances

PAPER

Cite this: *RSC Adv.*, 2015, **5**, 100905

Non-photolithographic plastic-mold-based fabrication of cylindrical and multi-tiered poly(dimethylsiloxane) microchannels for biomimetic lab-on-a-chip applications

Minjeong Jang,†[a] Young Jik Kwon*[bcde] and Nae Yoon Lee*[af]

Received 21st October 2015
Accepted 17th November 2015

DOI: 10.1039/c5ra22048c

www.rsc.org/advances

To overcome the limitations of conventional lithography for generating cylindrical and multi-tiered microchannels, we demonstrate a facile and alternative route for non-photolithographic fabrication of plastic molds *via* micro-milling combined with hot embossing. First, semi-cylindrical negative channels were engraved on poly(methylmethacrylate) (PMMA) using a ball mill, and the obtained semi-cylindrical negative channel structure was transferred onto poly(ethyleneterephthalate) (PET) *via* hot embossing performed at a temperature intermediate between the glass transition temperature (T_g) values of the two thermoplastics. In this way, a positive semi-cylindrical channel structure was formed on the PET without distorting the original patterns on the PMMA. The PET mold with positive structures was then replicated onto poly(dimethylsiloxane) (PDMS) to produce negative semi-cylindrical channels, and by aligning two identical PDMS replicas, a cylindrical microchannel with a completely circular cross section was formed. Second, multi-tiered channel structures were readily obtained by controlling the depths of the microchannels in the micro-milling process. The effectiveness of the fabricated cylindrical and multi-tiered microchannels was evaluated by constructing a microvascular network and human liver sinusoid structure as proof-of-concept experiments. The simple fabrication and high precision in the resulting structures will pave the way for the construction of disposable biomimetic Lab-on-a-Chip (LOC) platforms with low manufacturing cost in a simple and facile manner feasible for mass production.

1. Introduction

Lab-on-a-chip (LOC) systems[1,2] offer faster, parallel, and high-throughput biochemical analysis and screening on miniaturized platforms benefitting from reductions in sample volume, power requirements, and manufacturing cost. LOC systems together with microfluidic technology have greatly advanced many biological routines such as PCR,[3] cell manipulation,[4] and tissue engineering, to mention a few. Accordingly, numerous materials have been used, and material-specific fabrication techniques have been developed. Among these materials, the transparent poly(dimethylsiloxane) (PDMS) elastomer[5,6] has been widely utilized owing to its simple replica molding, easy surface modification, bonding feasibility, and excellent biocompatibility.

Most PDMS microdevices are typically fabricated *via* photolithography[7] followed by replica molding. Photolithography plays a pivotal role in the fabrication of a mold for subsequent pattern transfer onto a thermosetting PDMS prepolymer. Although photolithography can create microstructures with high resolution, it requires a bulky and expensive apparatus.[8] Besides the high fabrication cost, a photolithographically generated master mold provides micropatterns with rectangular cross-sectional morphologies.[9,10] Although microchannels with rectangular cross sections are easily fabricated and are quite versatile, there are still occasions when cylindrical microchannels with completely circular cross sections are desired. In particular, cylindrical microchannels are suitable for constructing microvasculature *in vitro* to mimic blood vessels,[11–15] conducting physiological cardiovascular flow analysis,[16] cell trapping,[17] or when homogeneous inner wall coatings must be added without generating dead

[a]*Department of BioNano Technology, Gachon University, 1342 Seongnam-daero, Sujeong-gu, Seongnam-si, Gyeonggi-do 461-701, Korea. E-mail: nylee@gachon.ac.kr; Fax: +82-31-750-8774; Tel: +82-31-750-8556*

[b]*Department of Pharmaceutical Sciences, University of California Irvine, 132 Sprague Hall, Irvine, CA 92697, USA. E-mail: kwonyj@uci.edu; Fax: +1-949-824-4023; Tel: +1-949-824-8714*

[c]*Department of Chemical Engineering and Material Science, University of California Irvine, Irvine, CA 92697, USA*

[d]*Department of Biomedical Engineering, University of California Irvine, Irvine, CA 92697, USA*

[e]*Department of Molecular Biology and Biochemistry, University of California Irvine, Irvine, CA 92697, USA*

[f]*Gachon Medical Research Institute, Gil Medical Center, Inchon, 405-760, Korea*

† Current address: Department of Bio and Brain Engineering, Korea Advanced Institute of Science and Technology, Daejeon, 305-701, Korea.

space. Also, rounded cross-sectional geometry is favorable for complete valve shutoff.[18] Cylindrical microchannels are also effectively used for sensing and detection purposes. Sochol *et al.*[19] fabricated circular-shaped microchannel for the precise docking of a single microbead to increase the diodicity performance of the microbead. Yoon *et al.*[20] fabricated circular cross-sectional microchannel for the identification of sinusoid in liver because the structure of the hepatic sinusoids affects diverse functions of the liver, and pathogen infection could alter morphology of sinusoid. For this reason, fabrication of microchannel mimicking human sinusoids could provide clues in the precise sensing and prediction of organ behavior. Recently, cylindrical microchannels have been fabricated by directly embedding cylindrical structures, for example, microwires,[21] metal wires,[15] nylon threads,[22] glass pipettes,[23] and sucrose fibers[24] into PDMS or by embedding optical fibers into negative photoresist.[25] These methods are inexpensive and can be used to form microchannels of various designs because of the flexibility of the microstructures. However, removal of the microstructures can be problematic, sometimes requiring the use of a mixed solvent to swell the molds afterward. Besides the above methods, injection of pressurized gas into a rectangular channel filled with the PDMS prepolymer,[17,26,27] direct solvent-assisted molding of PMMA solutions,[28] and the thermal reflow phenomenon[29] of photoresist have been used.

Similar to the fabrication of cylindrical microchannels, fabrication of multi-tiered microchannels is also challenging but necessary to ensure high performance of LOC devices. For example, multi-tiered microchannels have been used in many areas such as for constructing pillar structures for sorting techniques,[30–32] self-sorting of microbeads and cells by hydrophoresis,[33,34] blood cell separation,[35,36] micromixer application,[37,38] and for mimicking microvasculature.[11–13] The methods developed so far were typically realized by repeating photolithographic processes[39–42] or using electron beam or focused ion beam lithography.[43,44] Although multi-tiered features can be fabricated with high resolution, the fabrication takes a long time and requires precise alignment, making it unsuitable for fabricating complex structures.

Researchers have developed ways to fabricate microstructures non-photolithographically. For example, Zhao *et al.*[45] proposed a machining/reverse molding method to fabricate microfluidic channels with non-rectangular cross sections on poly(methylmethacrylate) (PMMA) by embossing with a metal mold. Wilson *et al.*[46] also proposed a similar concept to create microchannels with circular cross sections using a metal mold. Although high-precision micro-milling produces durable metal molds and sophisticated machining technique ensures mold fabrication in high resolution, the fabrication process takes a long time and is generally costly, which makes it inconvenient particularly when the design needs to be revised frequently.

Here, we demonstrate a facile alternative route for non-photolithographic fabrication of cylindrical and multi-tiered microchannels by fabricating thermoplastic mold by micro-milling and subsequently embossing the pattern onto a second thermoplastic. The mechanism of the embossing procedure is rooted in large difference in glass transition temperatures (T_g) between the two thermoplastics used. In this study, PMMA and poly(ethylene terephthalate) (PET) were used for the two thermoplastics, and the embossing temperature was controlled to be approximately intermediate between the T_g values of the thermoplastics. The effectiveness of the fabricated cylindrical and multi-tiered microchannels was evaluated by mimicking microvasculature, the smallest system of blood vessels in a body, and liver sinusoid structure, the smallest vessel in the liver which plays a critical role in the transportation of a small number of molecules to and from the blood stream, respectively.

2. Experimental

2.1 Materials

Poly(methylmethacrylate) (PMMA) ($T = 2$ mm) and poly(ethylene terephthalate) (PET) ($T = 2$ mm) were purchased from Goodfellow. Poly(dimethylsiloxane) (PDMS) silicone elastomer (Sylgard 184) and a curing agent were purchased from Dow Corning. Chelex 100 Molecular Biology Grade Resin ($D = 75$–150 μm beads) was purchased from Bio-Rad Laboratories. Computer numerical control (CNC) milling machine (TinyCNC-SC) was purchased from TINYROBO. End mills and ball mills were used to engrave channels. Custom-made pneumatic press machine was used for hot embossing. Oxygen plasma machine (Covance, Femto Science) was used for PDMS bonding. Human umbilical vein endothelial cells (HUVECs) and F-12K medium were purchased from ATCC. Fetal bovine serum (FBS) and trypsin–EDTA were purchased from Gibco, and heparin (sodium salt) was purchased from Santa Cruz. Triton X-100, endothelial cell growth supplement (ECGS), fibronectin (from human plasma), formalin solution (neutral buffered), and Dulbecco's phosphate-buffered saline (DPBS) were purchased from Sigma-Aldrich. Fluorescein isothiocyanate (FITC)-conjugated phalloidin was purchased from Enzo Life Science.

2.2 Fabrication of microdevice

Fig. 1 shows the overall procedures for plastic mold fabrication and PDMS replica molding for constructing cylindrical and multi-tiered PDMS microdevices. First, plastic molds featuring semi-cylindrical and multi-tiered microchannel structures were fabricated using a CNC milling machine equipped with ball mills ($R = 0.1$, 0.15, 0.25, and 0.5 mm) and end mills ($D = 0.2$, 0.3, 0.5, and 1.0 mm). Microchannels were engraved on a PMMA substrate ($T = 2$ mm) with a spindle speed of 13 500 rpm and feed speed of 30 mm s^{-1}. A flat PET substrate ($T = 2$ mm) was then placed atop the patterned PMMA mold, and the assembly was hot embossed using a custom-made pneumatic press machine at 85 °C under 0.1 MPa for 30 min. After the substrates were cooled, the assembly was physically detached. Next, the patterned PET was used as a mold, and its complementary patterns were transferred onto PDMS by replica molding. A 10 : 1 (w/w) mixture of PDMS prepolymer and the curing agent was degassed and poured onto the PET and then cured at 80 °C for 30 min. Holes were punched in the inlet and outlet ports for fluid

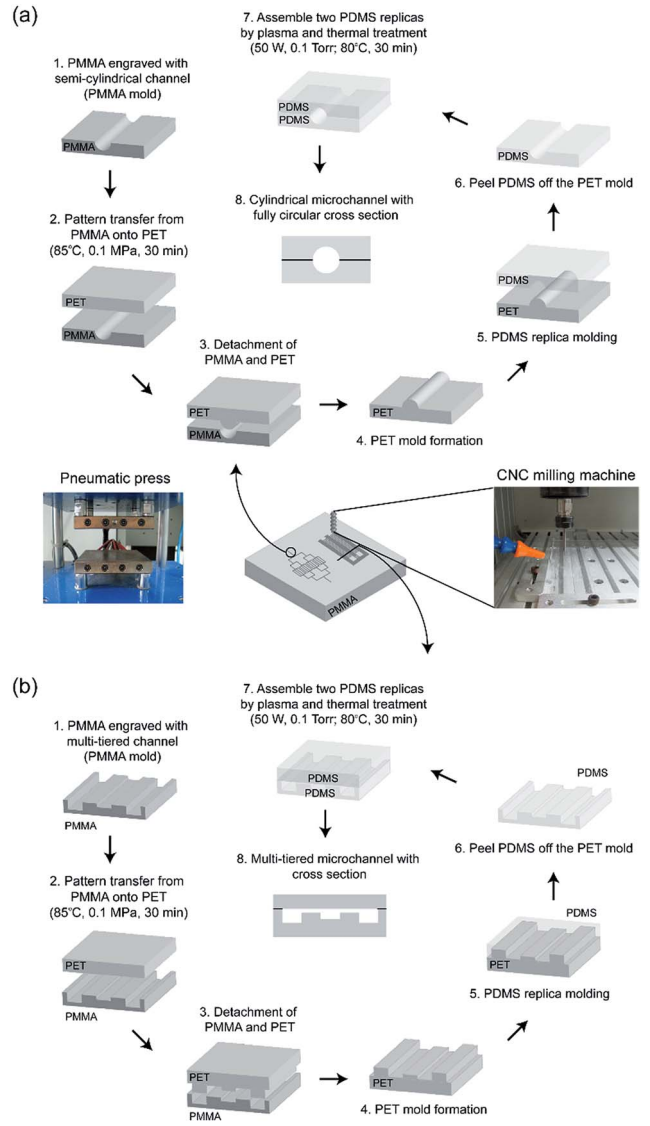

Fig. 1 Schematic of the fabrication of plastic molds and subsequent molding onto PDMS to fabricate (a) cylindrical and (b) multi-tiered microchannels.

introduction, and the two PDMS substrates were plasma treated (50 W, 0.1 Torr). Two PDMS replicas with identical semi-cylindrical microchannels were assembled in such a way that the semi-cylindrical microchannels faced each other and were aligned under a microscope and bonded at 80 °C for 30 min.

2.3 Analyses of microstructures and surface profiles

The microstructures and their cross-sectional profiles were observed using an inverted microscope (IX71, Olympus). Ink flow phenomena and microbead packing were observed under the inverted microscope.

2.4 Cell culture inside a microchannel

HUVECs were cultured in F-12K medium supplemented with 10% FBS, 0.1 mg mL^{-1} heparin, and 0.05 mg mL^{-1} ECGS, and were incubated in 5% CO_2 incubator at 37 °C. After this culture, the cells were treated with 0.25% trypsin–EDTA for 2 min for cell detachment, and then centrifuged for concentration and resuspension in the complete medium (supplemented F-12K medium). The PDMS microchannel was sterilized with 70% ethanol and exposed to UV overnight. The inside of the microchannel was coated with 1 mg mL^{-1} aqueous solution of fibronectin and reacted at 37 °C for 2 h. After the fibronectin coating, the microchannel was washed with DPBS, and HUVECs were introduced into the microchannel. After incubation in a 5% humidified CO_2 incubator at 37 °C for 20 min for cell attachment, the microchannel was reseeded with HUVECs and incubated, rotating the device by 90°.[26,29] This step was repeated to attach the cells on the entire surface of the microchannel. The microchannel was then incubated overnight. After incubation, cells were fixed with 5% neutral-buffered formalin for 15 min and permeabilized with 0.1% Triton X-100 for 10 min. Cells were stained with FITC-conjugated phalloidin, a staining dye for filamentous actin, for 40 min.[26,29]

3. Results and discussion

3.1 Surface profile analysis

Fig. 2 shows the surface profiles of both rectangular and semi-cylindrical microchannels engraved using the CNC milling machine. An end mill is defined by a tip with a flat bottom, whereas a ball mill is defined by a tip with a rounded bottom. Rectangular microchannels were fabricated on PMMA using end mills with diameters of 0.2, 0.3, 0.5, and 1.0 mm, resulting in various aspect ratios (depth : width) from 0.0625 (1 : 16) to 2 (2 : 1). Microchannels were then transfer-patterned onto PET by embossing at a temperature of approximately 85 °C, which is intermediate between the glass transition temperatures (T_g) of PMMA (T_g = 105 °C)[47] and PET (T_g = 65–80 °C).[48] The notably large difference in T_g values ensured successful transfer of the PMMA pattern onto PET without pattern melting or distortion.

Optical microscope (OM) images revealed that the PET replica (molds on the right side within the column with positive patterns) conformed to the negative patterns engraved on the PMMA mold (molds on the left side within the column) with high resolution when the aspect ratio of the pattern was relatively low. However, when the aspect ratio was increased, PET failed to precisely replicate the negative structure on PMMA because partially melted PET could not completely fill into the negative structure on PMMA, resulting in slightly rounded tips of the positive patterns generated on the PET. This was demonstrated by the results obtained for an aspect ratio of 2 : 1 when D = 0.2 mm, and for 1 : 2 when D = 1.0 mm. A multi-tiered microchannel is typically fabricated using rectangular microchannels. Based on the results shown in Fig. 2, we estimate that rectangular microchannels with aspect ratios of 1 or lower can be successfully replicated onto PET with reliable feature resolution, particularly when the diameter of the end mill is equal to or smaller than 0.5 mm. For the fabrication of semi-cylindrical microchannels, ball mills with radii of 0.1, 0.15, 0.25, and 0.5 mm were used. Unlike the case for the fabrication of rectangular microchannels, the ratio of radius to

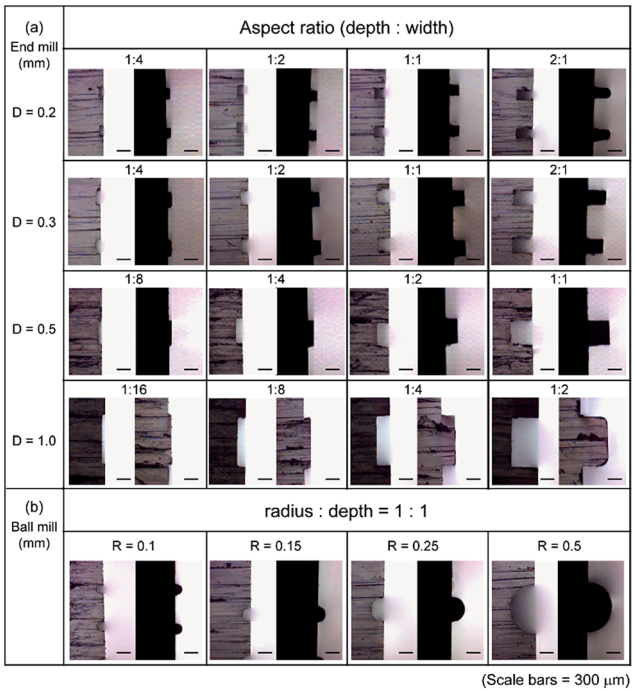

Fig. 2 Surface profiles of rectangular and semi-cylindrical microchannels engraved on PMMA using both end mills and ball mills with varying aspect ratios, which were subsequently embossed onto PET. Scale bars represent 300 μm. Molds on the left side within the column with negative patterns represent PMMA and those on the right side with positive patterns represent PET.

depth (radius : depth) was fixed to 1, because this ratio is critical for the fabrication of cylindrical microchannels with completely circular cross sections. OM images revealed that the negative patterns were engraved on PMMA with high resolution using ball mills, and positive patterns were precisely embossed onto PET regardless of the radii of the ball mills used.

3.2 Cylindrical microchannel mimicking a microvascular network

Fig. 3 shows digital camera and OM images of microfeatures mimicking human microvasculature formed by fabricating cylindrical microchannels on PDMS. The semi-cylindrical PDMS microchannels shown as (1)–(4) in Fig. 3(a) were created using ball mills with radii of 0.5, 0.25, 0.15, and 0.1 mm, respectively, with identical radius-to-depth ratios of 1. Fig. 3(b)–(e) show surface profiles of (1)–(4) in Fig. 3(a), respectively. The bonded PDMS assembly was sliced to examine the cross section after the bonding, and nearly complete circular cross sections were confirmed. Using this method, we fabricated cylindrical microchannels with completely circular cross sections ranging from 200 μm to 1 mm in diameter to mimic microvascular networks, particularly those of arterioles and venules (8 μm ≤ d < 250 μm)[49] as well as small arteries and small veins (250 μm ≤ d < 2 mm).[49] We also introduced red ink to verify the successful channel formation and check the bonding performance. By precisely controlling the size of the ball mill, we could also mimic arteries and the veins (d ≥ 2 mm) using our method, as

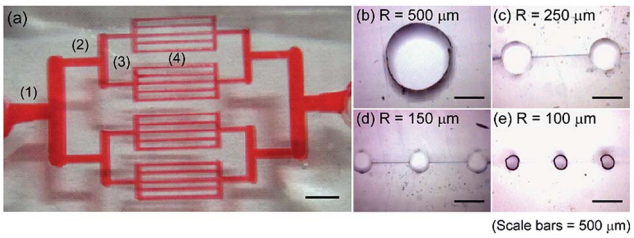

Fig. 3 (a) Digital camera image showing microchannels mimicking human microvascular network filled with red ink. (b)–(e) OM images showing the cross sections of the regions numbered as (1)–(4) in (a). Scale bars represent 500 μm.

well as capillaries (d < 8 μm).[49] The introduced fabrication process is fast, simple, and, most of all, highly inexpensive, and it requires no surface anti-adhesion treatment of the plastic mold, since PDMS is hydrophobic. The overall procedures for mold fabrication and PDMS replica molding took less than 3 h. In addition, the use of inexpensive plastic material allows flexible changes in the designs of microfeatures in the mold fabrication.

3.3 Multi-tiered microchannel mimicking human liver sinusoid

Fig. 4 shows a multi-tiered PDMS microchannel network mimicking the structure of human liver sinusoid on a chip[50,51] and its application as a filtration device. Multi-tiered microchannels are widely used for self-sorting of microbeads and cells by hydrophoresis[33,34] and for blood cell separation.[35,36] Multi-tiered microchannels can be readily fabricated on plastics using the CNC milling machine simply by programming different depth information as the end mills scan to form the desired microfeatures. Fig. 4(a) shows the design of the filtration device along with the direction of solution flow from the inlet toward the outlet while simultaneously flowing through the microfilter units. First, a PMMA mold with varying depth was fabricated. For example, a depth of 100 μm was used for the microchannel in the center for sample introduction, the depth was 150 μm for the microchannels on both margins for sample exit, and the depth was 40 μm for the perpendicular microfilter units interconnecting the inlet and outlet microchannels. The widths of the large channels fabricated for sample introduction and exit were identical at 1 mm, and that of the microfilter unit was 200 μm. Fig. 4(b) shows a digital camera image after ink introduction. No leakage was observed, and red ink was successfully introduced into the microfilter units. Fig. 4(c) shows an OM image of the region represented by (1) in Fig. 4(b). Chelex resin (D = 75–150 μm) was captured inside the inlet channel without leaking through the microfilter units. Although the width of the microfilter unit (200 μm) was slightly wider than the diameter of the Chelex resin used, resin did not leak out because of its physical aggregation, and only the solution was allowed to filter out.

Fig. 4(d)–(f) present OM images showing the original microfeatures engraved on PMMA, the primary pattern transferred from PMMA onto PET by hot embossing, and the secondary

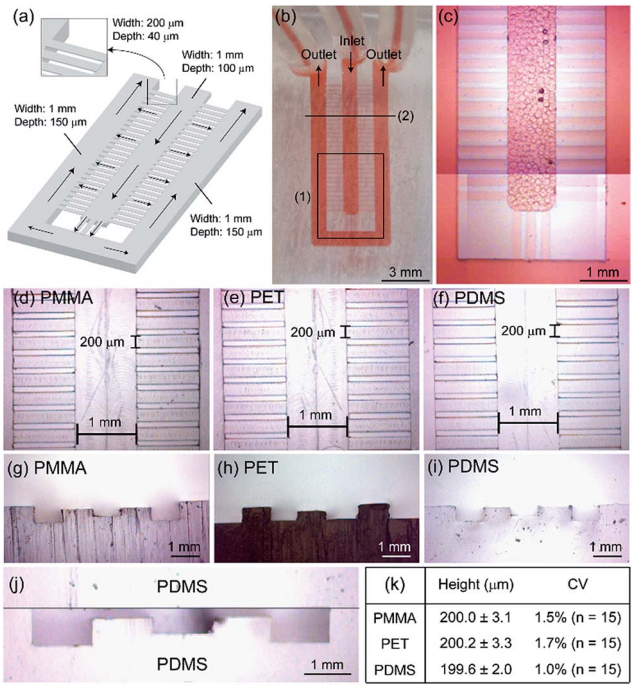

Fig. 4 (a) Schematic of the filtration device mimicking human liver sinusoid. (b) Digital camera image showing the overall microdevice. (c) Enlarged OM image of region (1) in (b) demonstrating successful packing of Chelex resin. (d–f) OM images of microfilter units fabricated on PMMA, PET, and PDMS. (g–i) OM images of cross sections along line (2) in (b), showing multi-tiered microchannels fabricated on PMMA, PET, and PDMS. (j) Cross section along line (2) in (b) after bonding two PDMS replicas. (k) Table showing the heights of microchannels shown in (d–f) and their CVs.

pattern transferred from PET onto PDMS by replica molding, respectively. Fig. 4(g)–(i) show the surface profiles along line (2) in Fig. 4(b) observed on the PMMA, PET, and PDMS, respectively. Multi-tiered microchannels were successfully transferred onto the successive substrates with high pattern fidelity. Fig. 4(j) shows the cross section of the multi-tiered, closed microchannel system obtained after bonding two PDMS replicas. The microfilter unit is clearly shown between the central inlet and marginal outlets. As shown in Fig. 4(d)–(i), the patterns finally formed on the PDMS were identical to those engraved on the PMMA because of the double replication. Even after double replication, the pattern exaggeration seemed negligible, as reflected by the almost identical sizes of the microfeatures formed on the PET and PDMS. Fig. 4(k) shows a table measuring the heights of the microchannels shown in (d–f) and their coefficients of variation (CVs) obtained by measuring the dimensions of 15 microchannels. The average heights of the microchannels fabricated on PMMA, PET, and PDMS were 200.0 ± 3.1, 200.2 ± 3.3, and 199.6 ± 2.0 μm, respectively, with corresponding CVs of 1.5%, 1.7%, and 1.0%. The fabrication process is simple and quick and ensures one-step fabrication of multi-tiered microchannel, which will allow wide applications in various LOC fields. Although PMMA and PET were used as the plastic materials for mold fabrication in this study, the method is not restricted to these two thermoplastics, and any two thermoplastics with notably different T_g can be utilized.

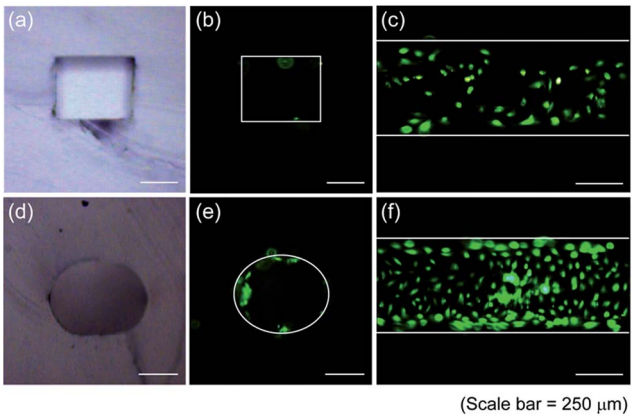

Fig. 5 (a) OM image of the cross section of a rectangular microchannel. (b) FM image of (a). (c) HUVECs growth inside a rectangular microchannel. (d) OM image of the cross section of a cylindrical microchannel. (e) FM image of (d). (f) HUVECs growth inside a cylindrical microchannel.

3.4 Cell growth inside rectangular and cylindrical microchannels

Fig. 5 shows the cell growth patterns inside rectangular (Fig. 5(a)–(c)) and cylindrical (Fig. 5(d)–(f)) PDMS microchannels. The same culture solution of HUVECs was introduced and HUVECs were grown along the inner walls of both types of microchannels to mimic a microvasculature. HUVECs played an important role as a model system to elucidate the regulation of endothelial cell functions in response to the external forces applied to the vessel wall. The cell staining results in the fluorescence microscopic (FM) images revealed that cells adhered more densely and homogeneously along the inner wall of cylindrical microchannel than they did inside a rectangular microchannel probably because of the curved morphology, characteristic of a cylindrical microchannel. Cell adherence seemed particularly inhibited along the corners of the rectangular microchannel, as represented by the low density of cells attached closer to the edges of the microchannel shown in Fig. 5(c). These results support the conclusion that cylindrical microchannels are more appropriate for cell growth, particularly when an *in vivo* system needs to be mimicked *in vitro*.

4. Conclusions

In this study, a simple, facile, and highly reproducible technique for the fabrication of cylindrical and multi-tiered PDMS microchannels using a plastic mold fabricated non-photolithographically was introduced. The plastic master mold was fabricated taking advantage of the notably large difference in T_g between the two thermoplastic materials utilized, and after the pattern transfer was repeated twice, the original pattern engraved on the first thermoplastic was copied in high resolution on PDMS *via* replica molding. The

fabricated cylindrical and multi-tiered microchannels successfully mimicked microvasculature and human liver sinusoid *in vitro*, as demonstrated by cell adhesion and growth experiments as well as resin packing experiments. Thus, this technique will pave the way for the construction of highly cost-effective and disposable biomimetic LOC sensor platforms suitable for mass production.

Acknowledgements

This research was supported by Basic Science Research Program through the National Research Foundation of Korea (NRF) funded by the Ministry of Science, ICT & Future Planning (2014R1A1A3051319) and the Public Welfare & Safety Research program through the National Research Foundation of Korea (NRF) funded by the Ministry of Science, ICT & Future Planning (NRF-2012M3A2A1051681). This research was also supported by 2015 SBS Foundation, Inc.

References

1 B. H. Weigl, R. L. Bardell and C. R. Cabrera, *Adv. Drug Delivery Rev.*, 2003, **55**, 349–377.
2 A. Nisar, N. Afzulpurkar, B. Mahaisavariya and A. Tuantranont, *Sens. Actuators, B*, 2008, **130**, 917–942.
3 I. Erill, S. Campoy, N. Erill, J. Barbé and J. Aguiló, *Sens. Actuators, B*, 2003, **96**, 685–692.
4 H. Andersson and A. van den Berg, *Sens. Actuators, B*, 2003, **92**, 315–325.
5 O. Hofmann, P. Niedermann and A. Manz, *Lab Chip*, 2001, **1**, 108–114.
6 H. Y. Tan, W. K. Loke and N.-T. Nguyen, *Sens. Actuators, B*, 2010, **151**, 133–139.
7 Q. Chen, G. Li, Q. H. Jin, J. L. Zhao, Q. S. Ren and Y. S. Xu, *J. Microelectromech. Syst.*, 2007, **16**, 1193–1200.
8 G. M. Whitesides, E. Ostuni, S. Takayama, X. Jiang and D. E. Ingber, *Annu. Rev. Biomed. Eng.*, 2001, **3**, 335–373.
9 M. J. Fuerstman, A. Lai, M. E. Thurlow, S. S. Shevkoplyas, H. A. Stone and G. M. Whitesides, *Lab Chip*, 2007, **7**, 1479–1489.
10 Y. Hongbin, Z. Guangya, C. F. Siong, W. Shouhua and L. Feiwen, *Sens. Actuators, B*, 2009, **137**, 754–761.
11 J. T. Borenstein, H. Terai, K. R. King, E. J. Weinberg, M. R. Kaazempur-Mofrad and J. P. Vacanti, *Biomed. Microdevices*, 2002, **4**, 167–175.
12 D. Lim, Y. Kamotani, B. Cho, J. Mazumder and S. Takayama, *Lab Chip*, 2003, **3**, 318–323.
13 D. R. Emerson, K. Cieslicki, X. Gu and R. W. Barber, *Lab Chip*, 2006, **6**, 447–454.
14 J. Borenstein, M. Tupper, P. Mack, E. Weinberg, A. Khalil, J. Hsiao and G. García-Cardeña, *Biomed. Microdevices*, 2010, **12**, 71–79.
15 S.-H. Song, C.-K. Lee, T.-J. Kim, I.-C. Shin, S.-C. Jun and H.-I. Jung, *Microfluid. Nanofluid.*, 2010, **9**, 533–540.
16 A. J. Calderón, Y. S. Heo, D. Huh, N. Futai, S. Takayama, J. B. Fowlkes and J. L. Bull, *Appl. Phys. Lett.*, 2006, **89**, 244103.
17 M. Abdelgawad, C. Wu, W. Y. Chien, W. R. Geddie, M. A. S. Jewett and Y. Sun, *Lab Chip*, 2011, **11**, 545–551.
18 N. J. Graf and M. T. Bowser, *Lab Chip*, 2008, **8**, 1664–1670.
19 R. D. Sochol, A. Lu, J. Lei, K. Iwai, L. P. Lee and L. Lin, *Lab Chip*, 2014, **14**, 1585–1594.
20 Y. J. Yoon, S. Chang, O. Y. Kim, B.-K. Kang, J. Park, J.-H. Lim, J. Y. Huang, Y.-K. Kim, J. H. Byun and Y. S. Gho, *PLoS One*, 2013, **8**, e68600.
21 Y. Jia, J. Jiang, X. Ma, Y. Li, H. Huang, K. Cai, S. Cai and Y. Wu, *Chin. Sci. Bull.*, 2008, **53**, 3928–3936.
22 M. K. S. Verma, A. Majumder and A. Ghatak, *Langmuir*, 2006, **22**, 10291–10295.
23 W. Jeong, J. Kim, S. Kim, S. Lee, G. Mensing and D. J. Beebe, *Lab Chip*, 2004, **4**, 576–580.
24 J. Lee, J. Paek and J. Kim, *Lab Chip*, 2012, **12**, 2638–2642.
25 L.-J. Yang, Y.-T. Chen, S.-W. Kang and Y.-C. Wang, *Int. J. Mach. Tool. Manufact.*, 2004, **44**, 1109–1114.
26 L. K. Fiddes, N. Raz, S. Srigunapalan, E. Tumarkan, C. A. Simmons, A. R. Wheeler and E. Kumacheva, *Biomaterials*, 2010, **31**, 3459–3464.
27 X. Yang, O. Forouzan, J. M. Burns and S. S. Shevkoplyas, *Lab Chip*, 2011, **11**, 3231–3240.
28 S. H. Lee, D. H. Kang, H. N. Kim and K. Y. Suh, *Lab Chip*, 2010, **10**, 3300–3306.
29 J. S. Choi, Y. Piao and T. S. Seo, *Bioprocess Biosyst. Eng.*, 2013, **36**, 1871–1878.
30 K. Cieslicki and A. Piechna, *Lab Chip*, 2009, **9**, 726–732.
31 J.-L. Li, D. Day and M. Gu, *Lab Chip*, 2010, **10**, 3054–3057.
32 N. Y. Lee, M. Yamada and M. Seki, *Anal. Bioanal. Chem.*, 2005, **383**, 776–782.
33 S. Choi and J.-K. Park, *Lab Chip*, 2009, **9**, 1962–1965.
34 S. Choi, S. Song, C. Choi and J.-K. Park, *Anal. Chem.*, 2009, **81**, 1964–1968.
35 V. VanDelinder and A. Groisman, *Anal. Chem.*, 2006, **78**, 3765–3771.
36 V. VanDelinder and A. Groisman, *Anal. Chem.*, 2007, **79**, 2023–2030.
37 Y. Du, Z. Zhang, C.-H. Yim, M. Lin and X. Cao, *Biomicrofluidics*, 2010, **4**, 024105.
38 A. D. Stroock, S. K. W. Dertinger, A. Ajdari, I. Mezic, H. A. Stone and G. M. Whitesides, *Science*, 2002, **295**, 647–651.
39 T. G. Leong, A. M. Zarafshar and D. H. Gracias, *Small*, 2010, **6**, 792–806.
40 H. Becker and C. Gärtner, *Anal. Bioanal. Chem.*, 2008, **390**, 89–111.
41 J. R. Anderson, D. T. Chiu, R. J. Jackman, O. Cherniavskaya, J. C. McDonald, H. K. Wu, S. H. Whitesides and G. M. Whitesides, *Anal. Chem.*, 2000, **72**, 3158–3164.
42 M. Y. Zhang, J. B. Wu, L. M. Wang, K. Xiao and W. J. Wen, *Lab Chip*, 2010, **10**, 1199–1203.
43 T. R. Groves, D. Pickard, B. Rafferty, N. Crosland, D. Adam and G. Schubert, *Microelectron. Eng.*, 2002, **61–62**, 285–293.
44 A. A. Tseng, *J. Micromech. Microeng.*, 2004, **14**, R15–R34.
45 D. S. Zhao, B. Roy, M. T. McCormick, W. G. Kuhr and S. A. Brazill, *Lab Chip*, 2003, **3**, 93–99.

46 M. E. Wilson, N. Kota, Y. T. Kim, Y. Wang, D. B. Stolz, P. R. LeDuc and O. B. Ozdoganlar, *Lab Chip*, 2011, **11**, 1550–1555.
47 C.-T. Lin, S.-W. Kuo, C.-F. Huang and F.-C. Chang, *Polymer*, 2010, **51**, 883–889.
48 R. B. Dupaix and M. C. Boyce, *Polymer*, 2005, **46**, 4827–4838.
49 J.-S. Lee, *Ann. Biomed. Eng.*, 2000, **28**, 1–13.
50 D. Huh, Y.-S. Torisawa, G. A. Hamilton, H. J. Kim and D. E. Ingber, *Lab Chip*, 2012, **12**, 2156–2164.
51 Y. Nakao, H. Kimura, Y. Sakai and T. Fujii, *Biomicrofluidics*, 2011, **5**, 022212.